We are IntechOpen, the world's leading publisher of Open Access books
Built by scientists, for scientists

4,800
Open access books available

122,000
International authors and editors

135M
Downloads

Our authors are among the

154
Countries delivered to

TOP 1%
most cited scientists

12.2%
Contributors from top 500 universities

CLARIVATE ANALYTICS
BOOK CITATION INDEX
INDEXED

WEB OF SCIENCE™

Selection of our books indexed in the Book Citation Index in Web of Science™ Core Collection (BKCI)

Interested in publishing with us?
Contact book.department@intechopen.com

Numbers displayed above are based on latest data collected.
For more information visit www.intechopen.com

5

NASICON Open Framework Structured Transition Metal Oxides for Lithium Batteries

[1]K.M. Begam, [2]M.S. Michael and [3]S.R.S. Prabaharan
Department of Electrical Engineering, Universiti Teknologi PETRONAS
Malaysia
Department of Chemistry, S.S.N. Engineering College, Chennai
India
Faculty of Engineering, The University of Nottingham
Malaysia

1. Introduction

Since the dawn of civilization, world has become increasingly addicted to electricity due to its utmost necessity for human life. The demand for electrically operated devices led to a variety of different energy storage systems which are chosen depending on the field of application. Among the available stationary power sources, rechargeable lithium-ion batteries substantially impact the areas of energy storage, energy efficiency and advanced vehicles. These batteries are the most advanced and true portable power sources combined with advantages of small size, reduced weight, longer operating time and easy operation. Such batteries can be recharged anytime (no memory effect) regardless of the charge current/voltage and they are reliable and safe. These unique features render their application in a variety of consumer electronic gadgets such as mobile phones, digital cameras, personal digital assistants (PDAs), portable CD players and palmtop computers. The high-end applications of this smart power source are projected for Hybrid Electric Vehicles (HEVs) as potential source of propulsion.

The evolution of rechargeable lithium batteries since their inception by Sony Corporation (Reimers & Dahn, 1992) has led to the development of new electrode materials (Kobayashi et al., 2000; Gaubicher, et al., 2000; Zhang et al., 2009; Zhu et al., 2008) for their effective operation in the real ICT environment. Among the new materials search for Li-ion batteries, polyanion compounds are growing into incredible dimensions owing to their intriguing properties (Manthiram & Goodenough, 1989; Huang et al., 2001; Yang et al., 2002; Chung et al., 2002).

In this chapter, we present a systematic study of a group of new polyanion materials, namely, lithium-rich [$Li_2M_2(MoO_4)_3$] and lithium-free [$Li_xM_2(MoO_4)_3$] (M= Ni, Co) phases of transition metal oxides having NASICON open framework structure. A simple and efficient approach to prepare the materials and a combination of characterization techniques to reveal the physical and electrochemical properties of these materials are covered at length. A separate section is devoted to a nano-composite approach wherein conductivity enhancement of all the four materials is enlightened. We begin this chapter with a brief

description of polyanion materials in general in general and NASICON structure type materials in particular.

2. Background

2.1 Polyanions

Despite the long known history of polyanion compounds as fast ion conductors or solid electrolytes (Goodenough et al., 1976; Hong, 1976), they relatively comprise a new category of electrode materials in recent times. The remarkable properties of these materials in tailor made compositions may lead them for use as electrodes in next generation lithium-ion batteries.

2.2 Types of polyanion compounds

Polyanion compounds incorporate NASICON structure type $Li_xM'_2(XO_4)_3$ and olivine type $Li_xM''XO_4$ materials.

NASICON materials are a family of compounds with $M'_2(XO_4)_3$ [M′ = Ni, Co, Mn, Fe, Ti or V and X = S, P, As, Mo or W] networks in which $M'O_6$ octahedra share all their corners with XO_4 tetrahedra, and XO_4 tetrahedra, share all their corners with $M'O_6$ octahedra (Manthiram & Goodenough, 1987). The interstitials and conduction channels are generated along the c-axis direction, in which alkali metal ions occupy the interstitial sites. Consequently, the alkali metal ions can move easily along the conduction channels (Wang et al., 2003). The $M'_2(XO_4)_3$ host framework is chemically versatile and it could be stabilized with a variety of transition metal cations M′ having an accessible redox potential and XO_4 polyanions. Such framework oxides were known to undergo a topotactic insertion/ extraction of a mobile atom due to the availability of an open three-dimensional framework (Nadiri et al., 1984; Reiff et al., 1986; Torardi & Prince, 1986) and hence are considered as electrode materials for rechargeable lithium batteries (Padhi et al., 1997).

The $Li_xM''XO_4$ [M′ = Fe, Co, Mn or Ni and X = P, Mo, W or S] olivine structure has Li and M′′ atoms in octahedral sites and X atoms in tetrahedral sites of a hexagonal close-packed (hcp) oxygen array. With Li in continuous chain of edge-shared octahedra of alternate planes, a reversible extraction/insertion of lithium from/into these chains would appear to be analogous to the two-dimensional extraction or insertion of lithium in the $LiMO_2$ oxides (Padhi et al, 1997).

2.3 NASICON type materials for energy storage– A brief history

Over the past, a number of researchers widely investigated NASICON structure type materials to facilitate exploitation in Li-ion batteries.

As early in 1984, lithium insertion/extraction properties of NASICON type polyanion compound, $Fe_2(MoO_4)_3$ was first reported by Nadiri et al. (1984). The compound was found to crystallize in monoclinic structure and it contains iron ions exclusively in 3+ state. It was shown that lithium could be inserted either chemically or electrochemically into the framework $Fe_2(MoO_4)_3$ with the concurrent reduction of ferric to ferrous ions (Fe^{3+} to Fe^{2+}) to form $Li_xFe_2(MoO_4)_3$ (x=2). The latter compound was found to crystallize in an orthorhombic structure (Nadiri et al., 1984; Reiff et al., 1986).

Pure $Fe_2(WO_4)_3$, isostructural with room temperature $Fe_2(MoO_4)_3$ (Harrison et al., 1985) could also reversibly insert lithium either chemically or electrochemically to form $Li_2Fe_2(WO_4)_3$ similar to $Li_2Fe_2(MoO_4)_3$. It was demonstrated that the voltage versus lithium content x for a $Li/Li_xFe_2(MoO_4)_3$ cell gives rise to a plateau in the 3 V region for $0<x<1.7$ substantiating the two-phase character of this compositional range. There was a sharp drop in V_{oc} at x=2.0 due to lattice disproportionation leading to irreversibility (Manthiram & Goodenough, 1987). This finding during the initial stage of exploring polyanions, in fact, formed a footing to further investigating this kind of compounds as electrode materials for lithium battery application.

Iron sulphate based positive electrodes, $Fe_2(SO_4)_3$ were shown to exist in hexagonal NASICON structure (Goodenough et al., 1976) as well as in a related monoclinic form (Long et al., 1979). Electrochemical insertion of lithium into both structure types was demonstrated by a two phase process in the range $0<x<2$ of nominal $Li_xFe_2(SO_4)_3$ giving rise to a flat voltage profile at 3.6 V versus a lithium metal anode. The end phase $Li_2Fe_2(SO_4)_3$ was confirmed to be orthorhombic. A difference of 600 mV in OCV observed between the sulfate and corresponding molybdate or tungstate systems is due to the influence of the counter cation on the Fe^{3+}/Fe^{2+} redox couple (Manthiram & Goodenough, 1989; Nanjundasamy et al., 1996). For x>2, there is a drop in voltage from the open circuit voltage (OCV). The performance of the material vitally depended on the initial phase of $Fe_2(SO_4)_3$ framework. The rhombohedral starting material retained modest capacity at lower current densities even after 80 cycles whereas the monoclinic $Fe_2(SO_4)_3$ showed a faster capacity fade (Okada et al, unpublished results). The overall performance of the hexagonal phase was shown to be superior to the monoclinic phase (Bykov et al., 1990).

Nanjundasamy et al. (1996) investigated the use of titanium, vanadium in the cation site and $(PO_4)^{3-}$ in the anion site to buffer $Fe_2(SO_4)_3$ against too large a drop in voltage and found that changing the polyanion group from $(SO_4)^{2-}$ to $(PO_4)^{3-}$ shifts the position of the redox couple from 3.2 eV to 2.5 eV for Ti^{4+}/Ti^{3+}, 2.5 eV to 1.7 eV for V^{3+}/V^{2+} and 3.6 eV to 2.8 eV for Fe^{3+}/Fe^{2+} below the Fermi level of lithium due to the smaller polarization of O^{2-} toward P^{5+} than toward S^{6+}. Each of these materials delivered a specific capacity of about 100 mAh/g between 2.0 and 4.2 V for a reversible insertion of two Li^+ per formula unit.

Padhi et al., (1998) noticed that the lithium insertion is accomplished by means of a single-phase reaction by tuning the position of the redox couple in the NASICON framework structures by anionic substitution as well. Electrochemical insertion of additional lithium into rhombohedral $Li_{1+x}Fe_2(SO_4)_2(PO_4)$ with NASICON framework over the range $0 \leq x \leq 1.5$ was found to be a reversible solid solution reaction within the hexagonal structure. The position of the redox couple Fe^{3+}/Fe^{2+} is located at 3.3 – 3.4 eV below the Fermi energy of lithium and this material delivered a reversible capacity of 110 mAh/g relative to a Li-metal anode.

In an independent analysis, $Li_3Fe(MoO_4)_3$ was shown to reversibly insert lithium down to 2 V akin to $Fe_2(MoO_4)_3$ (Dompablo et al., 2006). They conducted a comprehensive phase diagram study for $Li_{3+x}Fe(MoO_4)_3$ which revealed preservation of the structural framework for low lithium contents ($0<x<1$) ensuring good cyclability of the material in lithium cells, however, with a slight change of the cell volume (0.85%) (Vega et al., 2005).

Most of the above mentioned framework materials tend to operate in the low voltage range, which is not impressive for high voltage (>4 V) positive electrode application.

In the field of high voltage (>4 V) positive electrode materials, phosphate structures operating on the V^{3+}/V^{4+} receive increasing interest in view of the fact that the redox

potential and energy densities of phosphate-based polyanion compounds are as good as the current technologies (Padhi et al., 1997; Nanjundasamy et al., 1996) with good cycling properties at high scan rates (Nazar et al., 2002). Barker et al. (2003) explored $LiVFPO_4$ and Davies et al. (1994) investigated vanadium phosphate glasses as cathodes for Li-ion cells. A number of phases of $Li_3V_2(PO_4)_3$ were also studied as novel cathodes for Li-ion batteries. The removal of lithium is facile in such materials as they are structurally alike the NASICON family of materials. Amongst is the thermodynamically stable monoclinic form of $Li_3V_2(PO_4)_3$ which is isostructural to several other $Li_3M_2(PO_4)_3$ (M = Sc, Fe or Cr) materials (Huang et al., 2002; Yin et al., 2003). All three Li-ions may be reversibly removed from $Li_3V_2(PO_4)_3$ over two-phase electrochemical plateaus yielding a theoretical capacity of 197 mAh/g which is the highest for all phosphates reported so far. Nevertheless, electrochemical measurements showed that the material sustains reversibility when extraction/insertion is confined to two Li-ions with a reversible capacity of 130 mAh/g and the extraction of the third lithium is kinetically hindered and involves a significant over voltage (Saidi et al., 2002; 2003). Rhombohedral form of $Li_3V_2(PO_4)_3$ exhibits similar electrochemical characteristics as for the charge extraction, but reinsertion is limited to 1.3 lithium corresponding to 90 mAh/g of capacity (Gaubicher et al., 2000; Morcrette et al., 2003). Later, it was found that Zr substitution in orthorhombic $Li_3V_2(PO_4)_3$ phase enhances the electrochemical performance in terms of the discharge capacity and disappearance of the two-plateau boundary in the charge-discharge curves (Sato et al., 2000).
In 4 V class NASICON structure type materials explored to date, $Li_3Fe_2(PO_4)_3$ exits in monoclinic and rhombohedral forms. The $Fe_2(PO_4)_3$ framework remains intact under lithium extraction/insertion (Masquelier et al., 1996) occurring in a single continuous step giving rise to an initial discharge capacity of 115 mAh/g (Masquelier et al., 1998). This behavior slightly differs from $Li_3V_2(PO_4)_3$ where partial dissolution of vanadium takes place in deep reduction and at deep oxidation (Patoux et al., 2003).

3. Experimental processes

A succinct description of various experimental methods followed in the present study is presented in this section. In addition, the experimental procedure employed is highlighted wherever required.

3.1 Synthesis of open framework structured materials-Soft combustion technique

The soft-combustion technique offers several advantages over conventional high temperature and other low temperature methods. Materials prepared via the solid-state route contain two-phase mixtures due to the inhomogeneity caused by physical mixing of the raw materials. The particle morphology is often irregular and particle size is very large. On the other hand, the soft-combustion method, which is a low temperature preparative process is not time consuming and obviously well suited for bulk synthesis. Moreover, materials can be prepared with a single-phase structure and there is no impurity as second phase. Uniform particle morphology is an added advantage of this technique.
To prepare the polyanion transition metal oxides in the present study, starting materials such as lithium nitrate and hexa-ammonium heptamolybdate along with nitrate of the transition metals, Ni and Co were dissolved in deionized water in the appropriate molar ratio. The mixed solution was then added to an aqueous solution of glycine that acted as a

soft-combustion fuel. The quantity of glycine was optimized as twice the molar fraction of the starting materials. The solution was heated to boiling at 100 ^{o}C. A paste like substance formed was further heated at 250 ^{o}C to decompose the dried substance namely, the precursor. During the process of decomposition, the reaction was ignited by the combustible nature of glycine and gases like N_2O, NH_3 etc. were liberated leading to dry powders namely, the as-prepared material.

3.2 Characterization techniques employed

a. Physical characterization

As for the new materials prepared via the soft-combustion method, we employed physical characterization techniques such as X-ray diffraction (XRD) and scanning electron microscopy (SEM) analysis so as to find the crystallographic properties of the annealed samples and to observe the particle size distribution, shape and morphology features of the synthesized powder samples.

JEOL (model JDX 8030) and Rigaku (RINT-2500 V, 50 kV/100 mA, Rigaku Co. Ltd) X-ray diffractometers were used to record the diffractograms of the polyanion materials using CuKα radiation (λ=1.5406 Å). Peak locations and intensities were determined by a least-squares method and a refinement analysis, FullProof Suite, WinPLOTR 2004 was used to calculate the unit cells. We used Cambridge Instruments (Stereo scan S200) to collect SEM data for the family of new polyanion compounds. JEOL (JSM 6301F) was employed to study the high resolution images.

b. Electrochemical characterization

In order to elucidate the mechanism of lithium extraction/insertion in the new materials, and to generate kinetic and interfacial information, electrochemical studies were made, the details of which are given below.

i. Cyclic voltammetry (CV) measurements - Constant voltage cycling:

Cyclic voltammetry is an important and most commonly used electrochemical technique to characterize any electrochemical system. We examined the new materials by means of cyclic voltammetry studies and obtained information regarding the reversible nature (redox properties) of the materials and structural integrity during prolonged cycling with a view to validate the suitability of the materials for Li-ion batteries. We performed the Slow Scan Cyclic Voltammetry (SSCV) tests using Basic electrochemical system (BAS, Perkin Elmer, PARC model, USA) equipped with PowerCV® software.

ii. Galvanostatic (constant current) charge/discharge test:

Although potentiostatic experiments are a key in the sense that they readily divulge the reversibility of an electrode material, there are some applications for which a galvanostat is advantageous. The number of Li-ions participating in the redox reaction and hence the discharge capacity of the electrode material expressed in mAh/g is made known through Galvanostatic cycling test. In the present study, Arbin battery tester (Arbin instruments BT2000, USA) (8-channel unit) equipped with MITSPRO software was used to conduct the galvanostatic charge/discharge cycle tests.

iii. Electrode preparation and cell fabrication:

Teflon made two-electrode cells with SS current collectors were used to perform the electrochemical tests. Composite cathodes (positive electrodes) were prepared by mixing the electrode-active material [powders of polyanion materials], acetylene black and PTFE binder in a weight ratio of 80:15:5. The mixture was kneaded in agate type mortar and

pestle, rolled into thin sheets of around 100 ③m thick, and cut into circular electrodes of 3.14 cm^2 area and pressed onto an aluminum expanded grid mesh current collector. Test cells were composed of cathode (working electrode), a thin lithium foil (FMC, USA) as both counter and reference electrode and a microporous (Celgard® 3501 polypropylene) membrane soaked in a standard non-aqueous Li^+ electrolyte mixture solution (1M $LiPF_6$ in EC+DMC) (Merck LP 30) as a separator. The test cells were fabricated inside a glove box filled with high purity (99.999%) argon.

4. Results and discussion

4.1 Structure of $Li_2M_2(MoO_4)_3$

The crystal structure of $Li_2M_2(MoO_4)_3$ was determined using the CrystalDesigner® software. Figure 1 shows the polyhedral crystal structure of $Li_2M_2(MoO_4)_3$. The determination of the crystal structure revealed a three-dimensional framework consisting of metal-oxygen octahedra and trigonal prisms (where Li and M reside) which are interconnected by MoO_4 tetrahedra. The hexagonal motif of Mo tetrahedra around M octahedra joined by their faces is clearly seen in Fig. 1. Lithium atoms may occupy sites between or within the layers. The open framework allowed Li^+ ions to easily move in and out of the structure. Similar structures were already reported for analogous polyanion materials such as orthorhombic $Li_2Fe_2(MO_4)_3$ [M = Mo or W] (Manthiram & Goodenough, 1987).

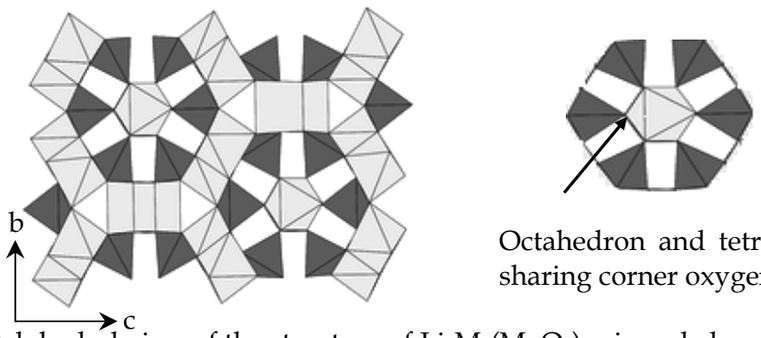

Fig. 1. Polyhedral view of the structure of $Li_2M_2(MoO_4)_3$ viewed along the (100) plane (Prabaharan et al., 2004).

4.2 Phase analysis

The phase purity of all the four materials was examined by means of XRD. In order to optimise the phase purity, we annealed the samples at different temperatures with a fixed soak time of 4h.

a. Lithium-rich phase of metal molybdates:

The XRD patterns of $Li_2Ni(MoO_4)_3$ recorded for the product annealed at 500°C exhibited some impurity peaks which were found to disappear upon annealing at 600°C and 700°C. In the case of the product annealed at 600°C, it was observed that the XRD peak positions are in good agreement with the preliminary crystallographic data previously reported (JCPDS #70-0452) indicating the formation of a well crystalline single-phase structure. So, the product annealed at 600°C was taken for further examination.

$Li_2Ni_2(MoO_4)_3$ was indexed in an orthorhombic structure with space group Pmcn. We used a refinement program (ICSD using POWD-12++) (Ozima et al., 1977) to calculate the cell

parameters of $Li_2Ni_2(MoO_4)_3$ and found the values as follows: a = 10.424(4) A°, b = 17.525(1) A° and c = 5.074(3) A°. It is to be mentioned here that no crystal structure information is available for $Li_2Ni_2(MoO_4)_3$ as for as we know except for the one available in JCPDS Ref. #70-0452. However, the latter pattern is non-indexed.

Although a single-phase structure with desired phase purity was formed at 600ºC/4 h/air, lithium could not be extracted from $Li_2Ni_2(MoO_4)_3$ during electrochemical charge owing to the difficulty in stabilizing nickel at a fixed valence state. It was suggested that a controlled oxygen atmosphere is essential during annealing of $LiNiO_2$ in order to stabilize nickel (Moshtev et al., 1995; Hirano et al., 1995). Accordingly, the as-prepared product of $Li_2Ni_2(MoO_4)_3$ was subjected to annealing at 600ºC/4h in the presence of oxygen atmosphere (90 ml/min). The XRD pattern of this product was recorded and compared with the one obtained under the same annealing conditions in ambient air.

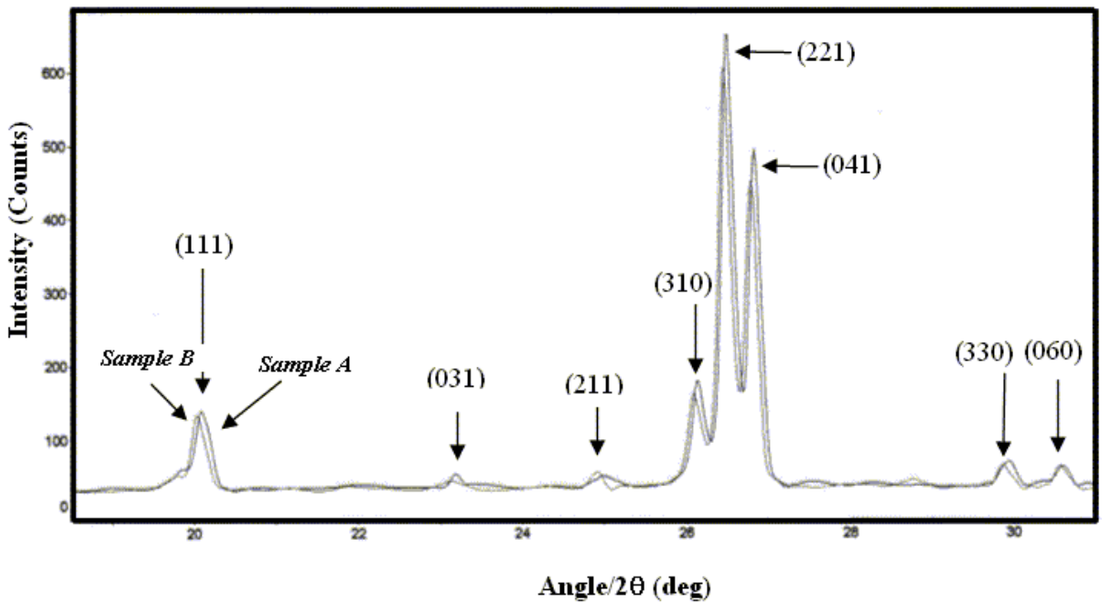

Fig. 2. Comparison of the peak positions of the diffractograms of as-prepared samples annealed in ambient air (sample A) and annealed in oxygen atmosphere (sample B) (Prabaharan et al., 2004).

Fig. 2 illustrates an expanded view of the differences in the peak positions of the chosen region with high intensity peaks (19˚-31˚/2θ angle) between the samples annealed in ambient air (sample A) and in oxygen atmosphere (sample B). A closer look at the diffractograms clearly reveals a slight but noticeable peak shift toward low 2θ regions for the sample B with respect to sample A, which is obviously a result of the heat treatment for the sample B in the presence of oxygen atmosphere. The peak shift is an indication of the volume change of the crystal lattice, which would probably facilitate the easy Li^+ extraction/insertion kinetics thereby improving the rate capability and discharge capacity compared to the one annealed in ambient air. The XRD pattern of $Li_2Co_2(MoO_4)_3$ is very much similar to that of $Li_2Ni_2(MoO_4)_3$. The disappearance of impurity peaks at a higher annealing temperature is well seen in figure 3. In addition, the peaks are refined and become sharper resulting in decreased crystallite size of the product. This is one of the favorable attributes for the effective utilization of $Li_2Co_2(MoO_4)_3$ positive-electrode active

powders. In the case of the product annealed at 600 ˚C, it was observed that the XRD peak positions are in good agreement with the crystallographic data previously reported (PDF # 31-0716), indicating the formation of a well crystalline single-phase structure.

$Li_2Co_2(MoO_4)_3$ was indexed in an orthorhombic structure with a space group Pnma. The refinement program used for $Li_2Ni_2(MoO_4)_3$ was used in this case as well and the lattice parameters were calculated to be a = 5.086(1) Å, b = 10.484(2) Å and c = 17.606(2) Å.

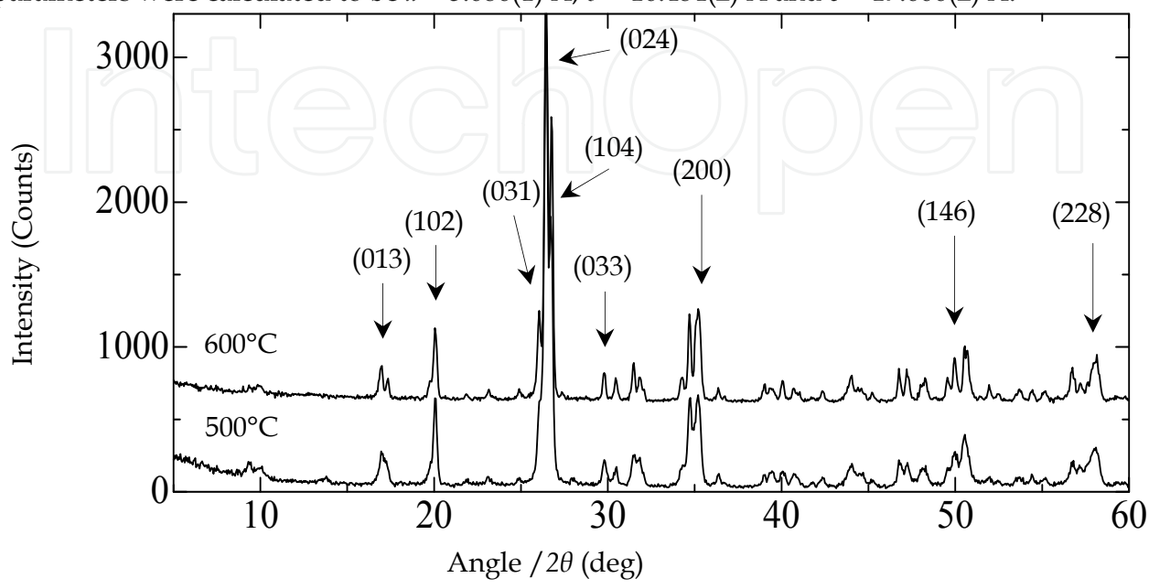

Fig. 3. XRD patterns of $Li_2Co_2(MoO_4)_3$ at (a) 500°C; (b) 600°C (Prabaharan et al., 2004).

b. Lithium-free phase of metal molybdates:

It is known from the XRD patterns of lithium-rich phases $Li_2M_2(MoO_4)_3$, that the appropriate annealing temperature to obtain single-phase polyanion materials is 600°C. Hence, the as-prepared product of $Ni_2(MoO_4)_3$ was annealed at 600 °C in the presence of oxygen atmosphere for two different annealing times, 4h and 7h to verify the effect of annealing time on the crystalline material.

Figure 4 presents the X-ray diffraction pattern of $Ni_2(MoO_4)_3$ annealed at 600°C for 4 h and 7 h in an oxygen atmosphere (90 ml/min). It is clear from the diffractograms that the peaks are alike in terms of peak position, sharpens of the peaks and intensity for the two samples indicating the formation of well crystalline structure. As the diffraction pattern is similar for both the samples, sample A was chosen for further investigation. The peaks were indexed using a least-squares refinement method.

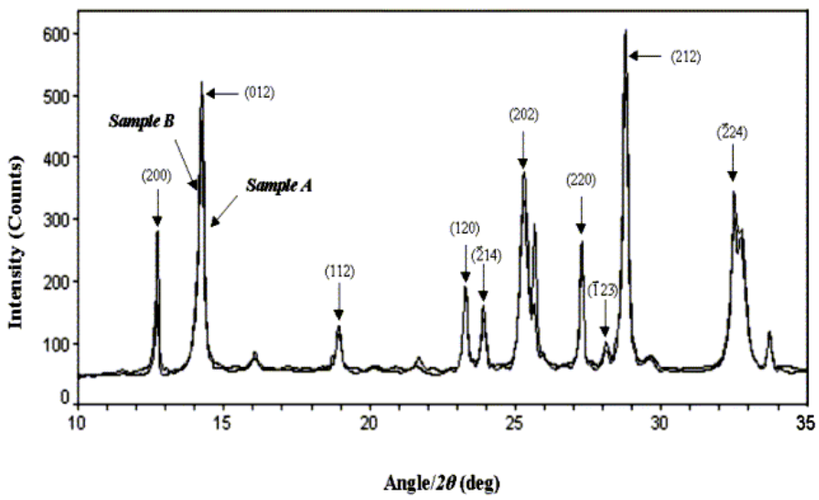

Fig. 4. X-ray diffractograms of $Ni_2(MoO_4)_3$ annealed at 600°C under O_2 purge (90 ml/min); Sample A - 600°C/4 h; sample B - 600°C/7h (Prabaharan et al., 2004).

The diffractograms of $Co_2(MoO_4)_3$ corresponding to 600°C and 700°C annealing temperature for 4 h signify the growth of peaks as shown in figure below (Fig. 5).
The peaks were indexed for the first time using a least-squares refinement method. $Co_2(MoO_4)_3$ was indexed in monoclinic structure with space group with P2/m. The lattice parameters were determined using a refinement program (FullProof Suite, WINPLOTR 2004) and calculated to be: a = 14.280(9) Å, b = 3.382(8) Å, c = 10.5571 Å and β = 117.9728˚.

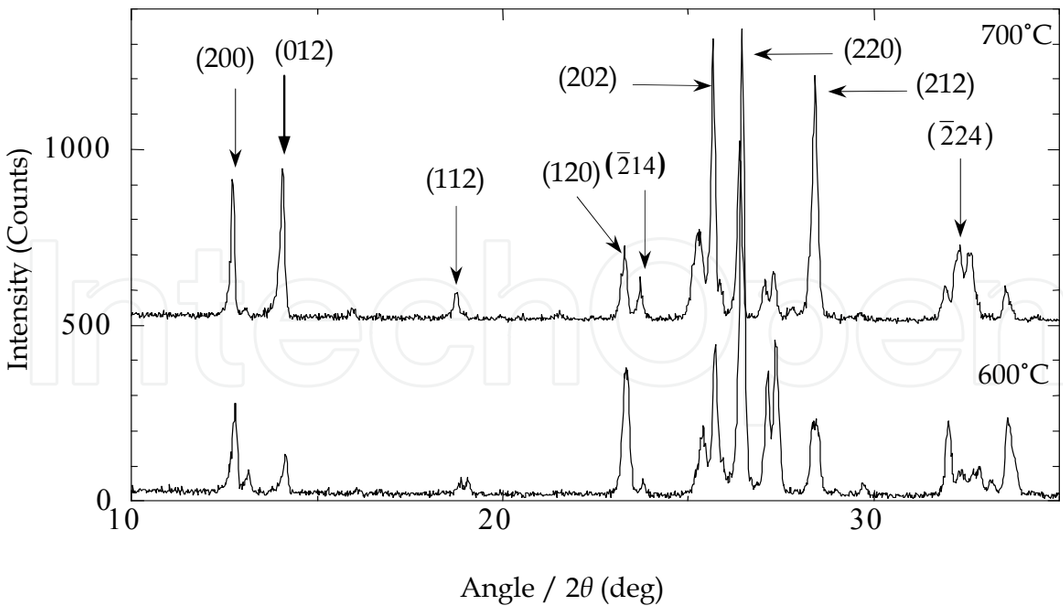

Fig. 5. X-ray diffraction patterns of $Co_2(MoO_4)_3$ annealed at 600 °C and 700 °C (Prabaharan et al., 2004).

4.3 SEM analysis

SEM images were recorded for the synthesized polycrystalline powders annealed at 600°C for 4h and are exhibited in Fig. 6. As for the lithium-rich phases ($Li_2Ni_2(MoO_4)_3$ & $Li_2Co_2(MoO_4)_3$, SEM reveals the formation fiber-like grains with controlled grain growth and morphology (Fig. 7a & b). In both cases the particles are loosely agglomerated with the average size within the submicrometre range.

As for as the morphology is concerned, $Ni_2(MoO_4)_3$ as well as $Co_2(MoO_4)_3$ powders exhibit uniform and ultrafine spherical grains (Fig. 7 c & d) with nearly uniform particle size. The inset in Fig. 7c shows the SEM picture recorded at high magnification to unveil the actual grain size distribution. Consequently, the micrograph (inset) demonstrates nanosized spherical grains with a single grain size of ~100nm. From the nanostructure morphology of $Co_2(MoO_4)_3$ as depicted in Fig. 7d, it is readily observed that $Co_2(MoO_4)_3$ powders contain uniform spherical grains of much reduced size (20 nm) when compared to $Ni_2(MoO_4)_3$.

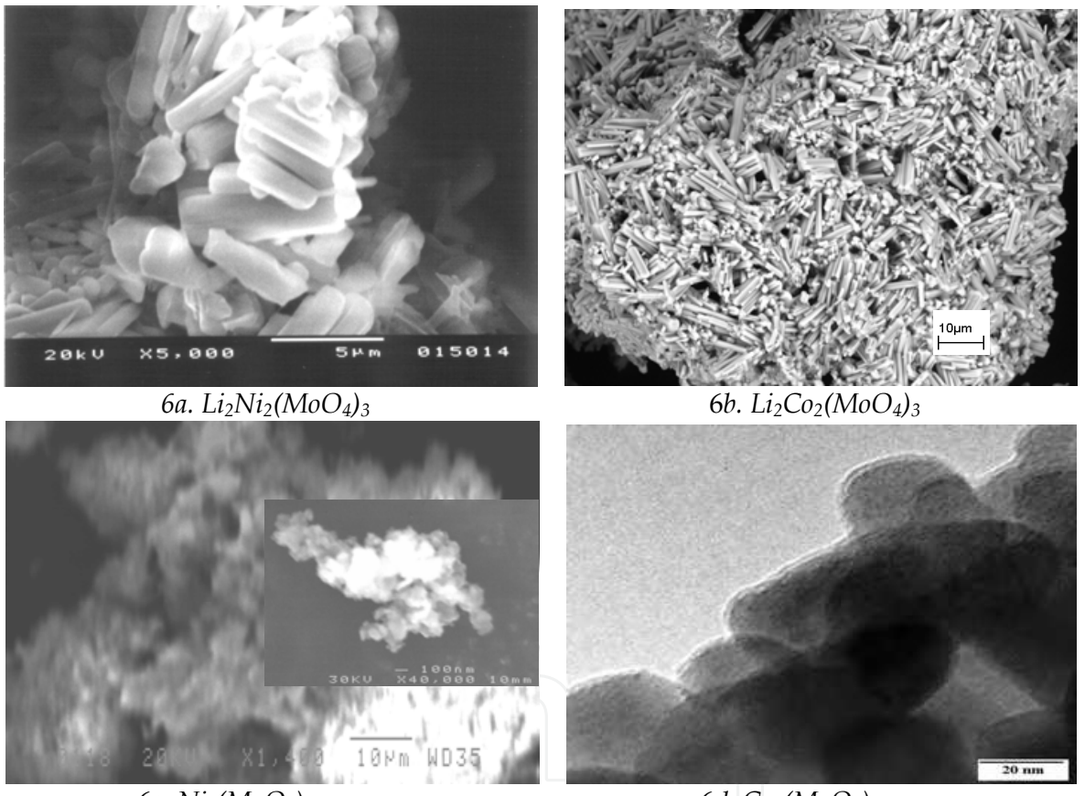

6a. $Li_2Ni_2(MoO_4)_3$ *6b. $Li_2Co_2(MoO_4)_3$*

6c. $Ni_2(MoO_4)_3$ *6d. $Co_2(MoO_4)_3$*

Fig. 6 (a, b & c). SEM images; d. TEM image. (Prabaharan et al., 2004, 2006, 2008).

4.4 Electrochemical studies

a. Cyclic voltammetry (CV) measurements

In order to elucidate the electrochemical reversible nature of the materials taken for the present investigation, we carried out cyclic voltammetry tests on $Li/Li_2M_2(MoO_4)_3$ and $Li/Li_xM_2(MoO_4)_3$ half cells at a low scan rate (0.1 mV/s). The cells were first charged to extract lithium from the host materials and then discharged to insert lithium in the host structures. We discovered that all the four materials possess electrochemical reversibility

with regard to Li^+ extraction/insertion. Accordingly, Fig. 7 presents the slow scan cyclic voltammograms of $Li_2M_2(MoO_4)_3$ composite electrodes vs. Li/Li^+ cycled between 4.9 V and 1.5 V. It is clearly seen from the CV profiles that $Li_2M_2(MoO_4)_3$ polyanion materials reveal a systematic evidence for the electrochemical reversibility through the oxidation and reduction peaks corresponding to the two transition metal ions, M^{2+} [M = Ni, Co] and Mo^{6+}. As for the electrochemical reversibility of $Li_2M_2(MoO_4)_3$ vs. Li/Li^+, during charge (anodic scan), we observed the first oxidation of Ni^{2+}/Ni^{3+} at 4.4 V whilst the oxidation of Co^{2+}/Co^{3+} was found to occur at 4.3 V. Following the charging process, during discharge, (cathodic scan), we were able to notice a single peak at 3.2 V corresponding to Ni^{3+}/Ni^{2+} reduction, and its analogous counterpart, Co^{3+} was found to reduce to Co^{2+} at 3.1 V. The shift in the redox potential of M^{3+}/M^{2+} is correlated to the polyanion $(MoO_4)^{2-}$ in the host framework structure. In fact, we emphasized this point in some of our publication (Prabaharan et al., 2004) as reported by Nanjundaswamy et al. (1996), who studied the effect of NASICON-related framework compounds such as $M_2(SO_4)_3$ and $Li_xM_2(PO_4)_3$

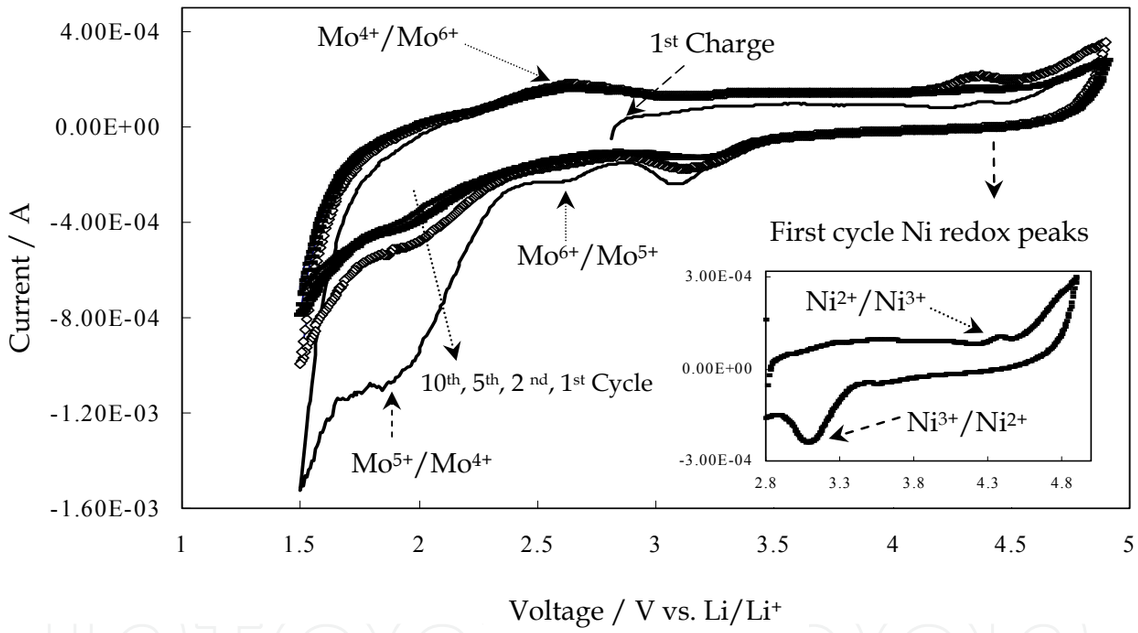

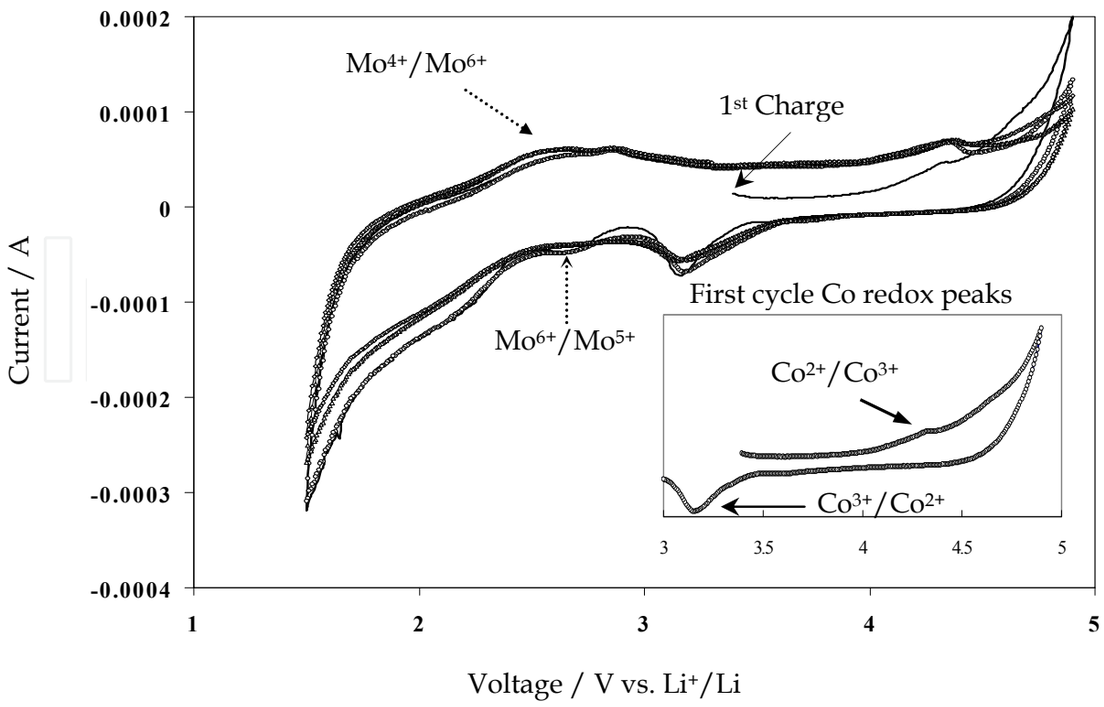

Fig. 7. Slow scan cyclic voltammetry of $Li_2M_2(MoO_4)_3$ vs. Li/Li^+. Scan rate: 0.1 mV/s; V_{max}: 4.9 V (oxidation); V_{min}: 1.5V (reduction); Inset: First cycle Ni/Co redox peaks (Prabaharan et al., 2004).

(M= transition metal) in the context of how a change in the polyanion group shifts the redox potentials of the M cations and the influence on the Li^+ insertion rate and cyclability of end member phase transitions of the lithiated and delithiated phases.

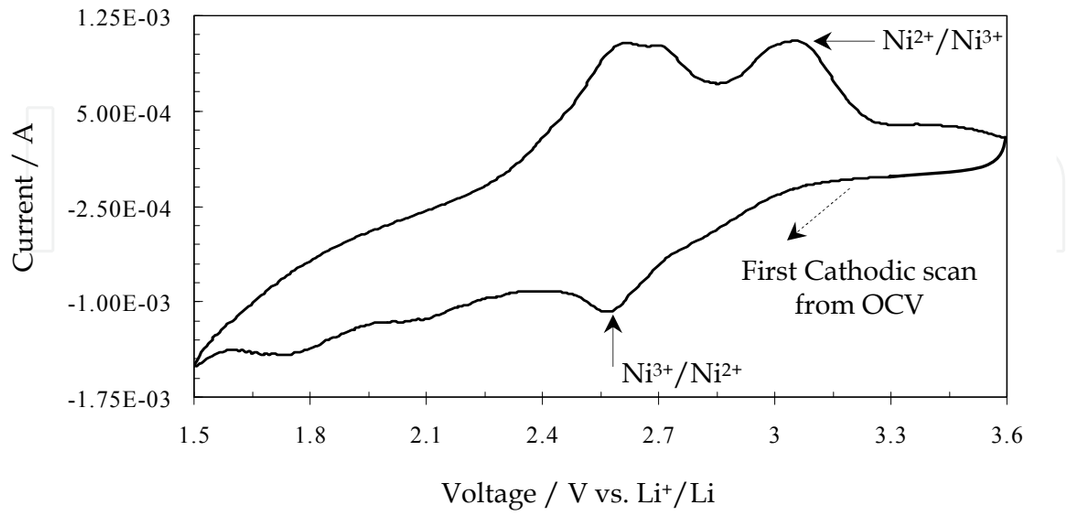

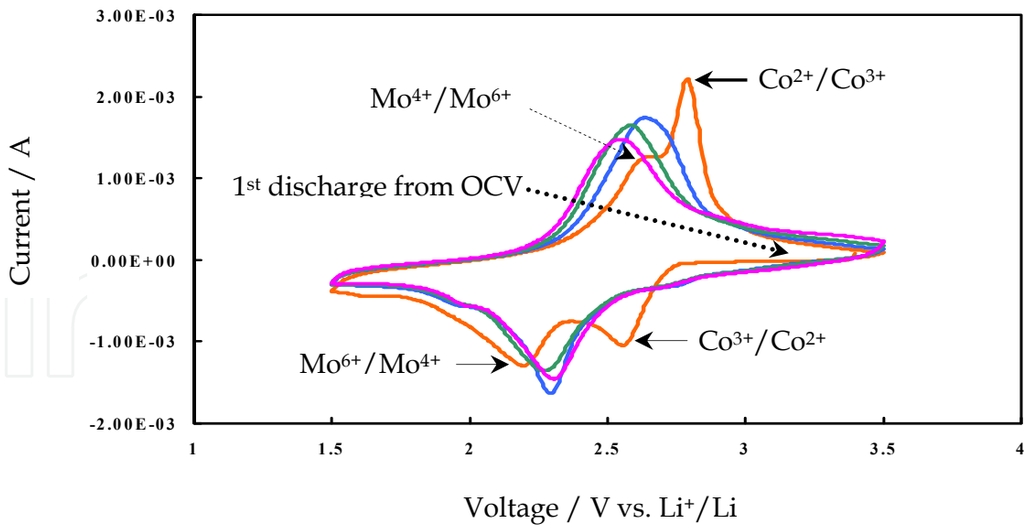

Fig. 8. Slow scan cyclic voltammetry of $Li_xM_2(MoO_4)_3$ vs. Li/Li^+. Scan rate: 0.1 mV/s; V_{max}: 3.6/3.5 V (oxidation); V_{min}: 1.5V (reduction). (Prabaharan et al., 2004, 2006).

During the continuation of the reduction process down to 1.5 V, two peaks were noticed at 2.6 and 1.9 V in the case of $Li_2Ni_2(MoO_4)_3$ and at 2.6 and 2 V for $Li_2Co_2(MoO_4)_3$ indicating the reduction of Mo^{6+} to Mo^{5+} and Mo^{4+}. During successive cycling, these two peaks were found to merge into a single broad peak in both cases, implying the slow and steady dynamics of Li^+ into the active material. Upon further cycling, we were able to observe a broad anodic peak at 2.6 V representing the Mo oxidation, followed by a high voltage peak at 4.3 V indicating the oxidation of M^{2+} cations back to 3+ state.

The slow scan cyclic voltammograms of $Li_xM_2(MoO_4)_3$ composite electrodes vs. Li/Li^+ cycled between 1.5 V and 3.6 V [for $Li_xNi_2(MoO_4)_3$] and between 1.5 V and 3.5 V [for $Li_xCo_2(MoO_4)_3$] are shown in Fig. 8. The cells were first discharged to insert lithium in $M_2(MoO_4)_3$ framework structure and then charged to extract lithium. The CV profiles demonstrate the electrochemical reversibility of the material and exhibits the reduction and oxidation peaks corresponding to the two transition metal ions M^{3+} and Mo^{6+}.

During the first discharge from OCV, the reduction of M^{3+}/M^{2+} was observed at 2.6 V and as the reduction process continues down to 1.5 V, two other broad peaks were observed at 2.1 V and 1.7 V in the case of $Li_xNi_2(MoO_4)_3$ due to the reduction of Mo^{6+} (to its lower oxidation states). On the other hand, a single reduction peak was observed at 2.2 V for $Li_xCo_2(MoO_4)_3$ indicating two-electron transfer during Mo^{6+} reduction. Upon the first charge after discharge, in lithium-free nickel molybdate, oxidation of Mo back to its higher oxidation state (6+ state) and Ni^{2+}/Ni^{3+} transitions were noticed at 2.6 V, 2.7 V and 3.1 V respectively. Whereas, in lithium-free cobalt molybdate Mo^{4+}/Mo^{6+} transition was observed in a single step at 2.65 V which was followed by oxidation of Co^{2+} to Co^{3+} at 2.8 V. These observations are similar to $Li_2M_2(MoO_4)_3$ except for a slight change in the position of the peaks and peak height. The same trend was observed during extended cycling.

Furthermore, in all the four cases, oxidation and reduction of M and Mo ions (cations and counter cations) were clearly observed during prolonged cycling. The excellent electrochemical reversibility of the new materials as evidenced from the CV profiles is an indication of the appropriateness of the new materials for application in rechargeable

lithium batteries. With a view to strengthen our findings from CV studies, we performed charge/discharge tests galvanostatically, the details of which are given in the next section.

b. Galvanostatic charge/discharge test

We conducted charge/discharge tests on the $Li_2M_2(MoO_4)_3$/Li half-cells between 4.9 and 1.5 V at low current densities: 2.5 mA/g (charge) and 1.25 mA/g (discharge). $Li_xM_2(MoO_4)_3$/Li half-cells were subjected to discharge/charge test against lithium in half-cells between 1.5 and 3.5 V at low current densities: 2.5 mA/g (discharge) and 10 mA/g (charge). From the galvanostatic charge/discharge tests conducted for the first 20 cycles, we calculated the number of Li-ions participated in the electrochemical redox reactions from the amount of electrical charges spent as a function of elapsed time on the tests and hence the discharge capacity of the polyanion electrode materials.

Fig. 9 represents the galvanostatic multiple charge-discharge curves of the half-cell $Li_2Ni_2(MoO_4)_3$/Li. It was observed that the first charge curve from OCV (2.8 V) exhibit a smooth plateau with an onset at about 4.6 V, which extends steadily with an increasing trend up to 4.9 V vs. Li/Li^+. During the first charge process of lithium extraction, one Li^+ per formula could be extracted with a charge capacity of 45 mAh/g as shown in Fig. 9. During the first discharge, 2.6 Li^+ per formula unit could be reversibly inserted down to 1.5 V with a discharge capacity of ~ 115 mAh/g. The transitions of $Ni^{3+}$to Ni^{2+} and Mo^{6+} to its lower oxidation states are visible as two-step discernible plateaus during the first discharge. These findings are consistent with the first cycle reduction peaks obtained from SSCV studies.

Even though the compound exhibited a good high voltage charge profile during the first lithium extraction, the discharge profile demonstrated poor reduction kinetics during the beginning of discharge (insertion) between 4.9 and 3.0 V. Besides this, the electrochemical insertion was limited to 0.25 lithium per formula unit between 4.9 and 2.5 V vs. Li/Li^+. This poor rate kinetics is strongly attributed to the inherent structural limitation as well as poor electronic conductivity, which is common for polyanion materials reported so far (Goodenough et al., 1997; Tarascon and Armand, 2001). Moreover, once Mo^{6+} in tetrahedral site is reduced to Mo^{5+} or Mo^{4+}, it may be difficult to oxidize it back keeping the same crystal structure, and this partly explains the poor cyclability of $Li_2Ni_2(MoO_4)_3$. It was observed that there is no change in the shape of the charge and discharge profiles after the first cycle indicating the structural stability of the host material during repeated cycling. However, there is a continuous decreasing trend in terms of the amount of Li^+ inserted into $Li_2Ni_2(MoO_4)_3$ as the cycle number increases for obvious reasons. This leads to a considerable decline in the discharge capacity of the material.

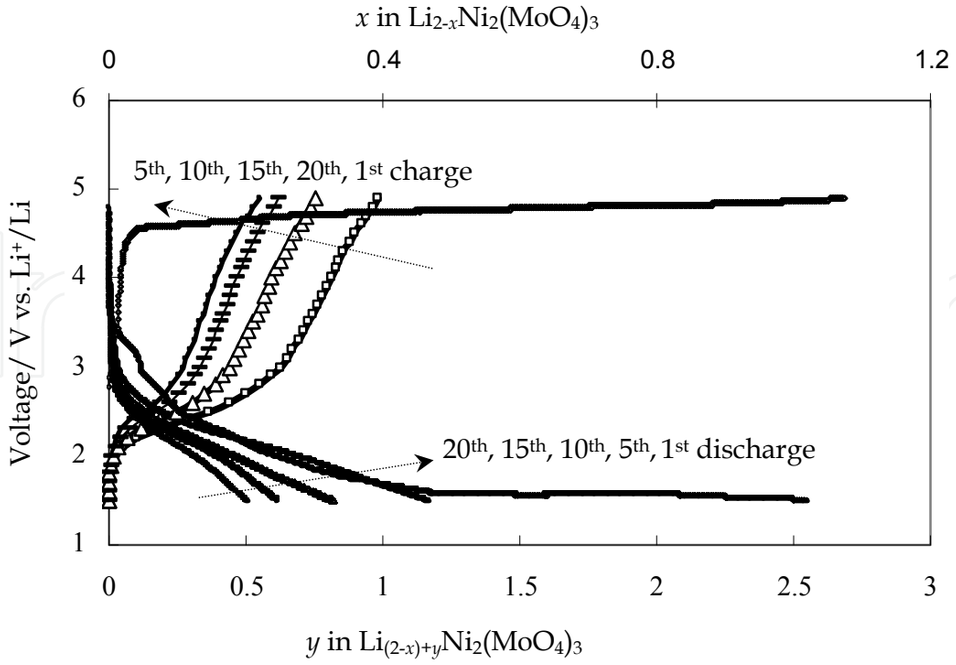

Fig. 9. Multiple charge/discharge curves of $Li_2Ni_2(MoO_4)_3$//Li cell between 4.9 and 1.5 V

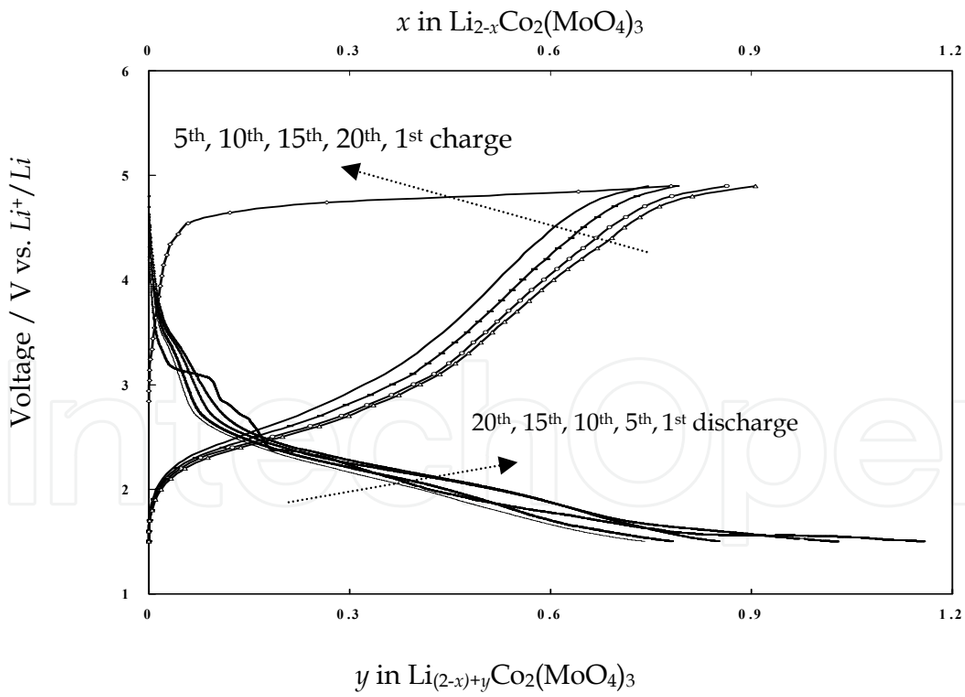

Fig. 10. Multiple charge/discharge curves of $Li_2Co_2(MoO_4)_3$//Li cell between 4.9 and 1.5 V (Prabaharan et al., 2004).

The galvanostatic multiple charge-discharge curves of the half-cell $Li_2Co_2(MoO_4)_3$/Li are shown in the following figure (Fig. 10). It is clearly seen from Fig. 10 that the

charge/discharge profiles are comparable to Fig. 9 with regard to shape, oxidation and reduction of Co^{2+} and Mo^{6+} although a slight difference was noticed in the first charge and discharge capacity values; first lithium extraction process corresponds to 0.8 Li^+ per formula leading to a charge capacity of 35 mAh/g and 1.2 Li^+ per formula unit could be reversibly inserted down to 1.5 V with a discharge capacity of ~ 55 mAh/g. Nevertheless, the performance of the cobalt-containing polyanion compound was found to be better with regard to extended cycling than its analogous nickel counterpart despite their similar structural environment. Although the extended cycling characteristics are rather better, still the material suffers from poor rate kinetics for the reasons explained above.

The galvanostatic multiple discharge-charge curves of $Ni_2(MoO_4)_3$/Li half-cells are shown in Fig. 11. It was observed that the first discharge curve from OCV (3.4 V) exhibited a sloping plateau corresponding to the reduction of nickel followed by a perceptible plateau due to the reduction of molybdenum. These observations are in good agreement with the reduction peaks found in CV studies (Fig. 8). During the first discharge process of lithium insertion down to 1.5 V, 3.6 Li^+ could be inserted which amounts to a discharge capacity of ~ 170 mAh/g. During the first charge (extraction) after discharge, 3 Li^+ per formula unit could be extracted up to 3.5 V with a charge capacity of ~ 135 mAh/g. The discharge capacity was found to slowly deteriorate upon repeated cycling similar to what was observed in the case of $Li_2M_2(MoO_4)_3$. We ascertained this as due to loss of structural integrity of the electrode-active material originating from the number (x>2) of lithium inserted in the host structure. Here it is recalled that such an effect was earlier observed in the case of an analogous material, $Li_xFe_2(XO_4)_3$ which also suffered from structural phase transition (monoclinic to orthorhombic) owing to the above mentioned cause (Manthiram and Goodenough 1987).

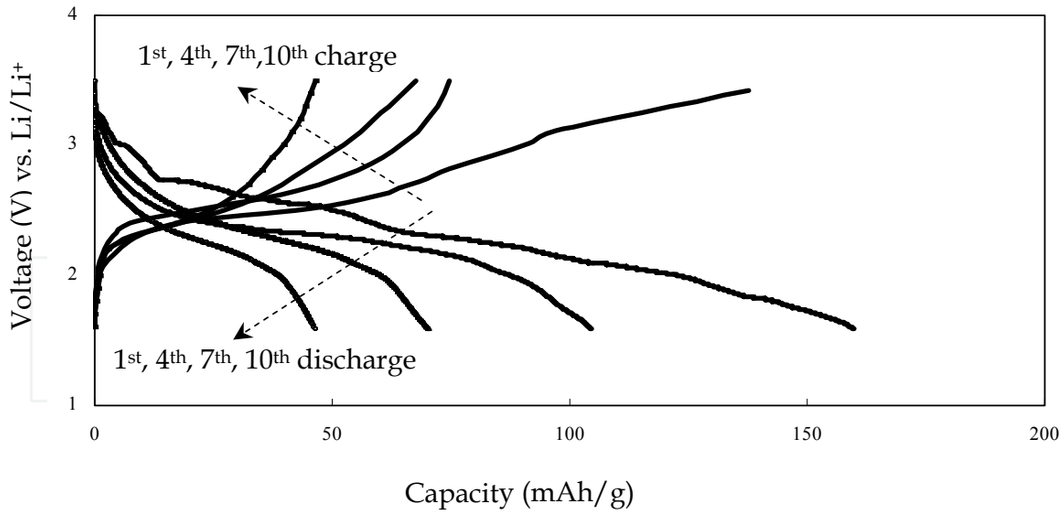

Fig. 11. Multiple discharge/charge curves of $Li_xNi_2(MoO_4)_3$//Li cell between 3.5 and 1.5 V (Prabaharan et al., 2004).

As for the half-cell $Li_xCo_2(MoO_4)_3$/Li, Fig. 12 shows the multiple discharge/charge curves. The first discharge process of Li^+ insertion began at 3.4 V (OCV) and only negligible amount of Li^+ could be inserted into $Co_2(MoO_4)_3$ until the potential decreased to 2.7 V from where the discharge curve exhibited two plateaus centered at approximately 2.6 V and 2.2 V.

These plateau regions correspond to the reduction of cobalt (Co^{3+}/Co^{2+}) and molybdenum (Mo^{6+}/Mo^{5+}) respectively. During the first discharge, ~ 2.4 Li^+ per formula unit could be inserted down to 1.5 V leading to a discharge capacity of ~ 110 mAh/g. During the first charge after discharge, 1.7 Li^+ could be extracted up to 3.5 V with a charge capacity of ~ 75 mAh/g. It is seen from Fig. 12 that the two plateau regions present during the first discharge disappeared and discharge/charge after the first cycle showed consistent potential profiles over the potential window of 3.5 – 1.5 V. These observations corroborate our findings from CV studies (Fig. 8). It is evident from Fig. 12 that the amount of lithium inserted into $Co_2(MoO_4)_3$ decreases slowly as the cycle number increases as observed in all the previous three cases for well-known reasons.

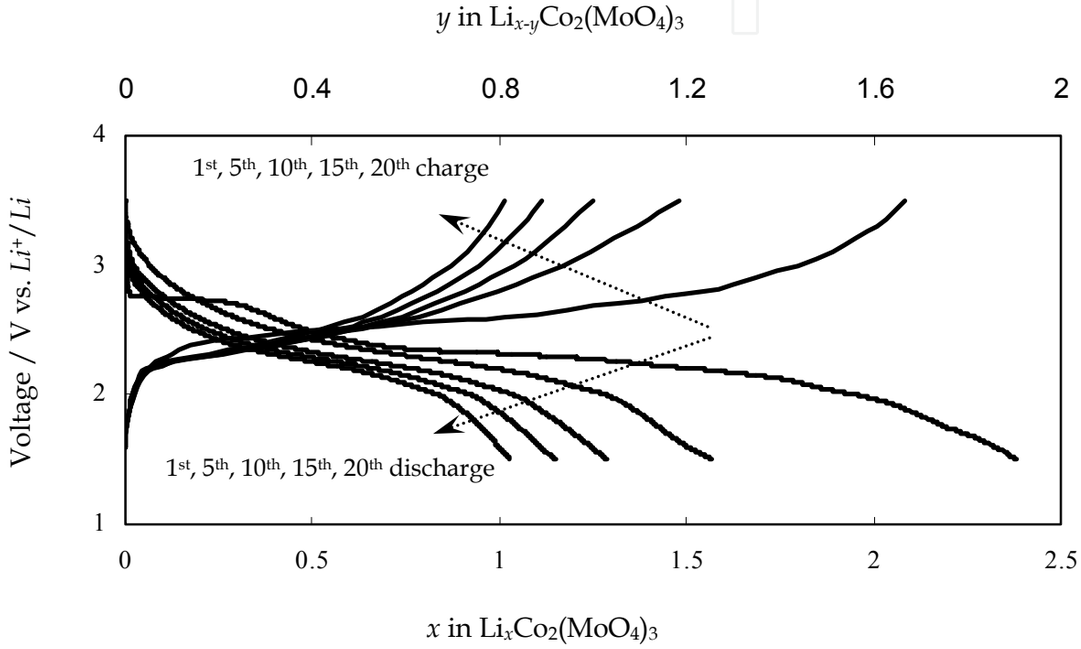

Fig. 12. Multiple discharge/charge curves of $Li_xCo_2(MoO_4)_3$//Li cell between 3.5 and 1.5 V

4.5 Limitations in using polyanion materials for lithium batteries

Although the polyanion materials examined in the present study exhibit reversible electrochemical lithium extraction/insertion properties over a considerable number of cycles, all of them invariably suffer from very low electronic conductivity which stems from their insulating nature. This ultimately resulted in poor capacity retention during prolonged cycling. As a consequence, the window of opportunity for this group of materials to be used in rechargeable lithium batteries is narrowed down.

We rectified this complexity successfully by means of a nano-composite approach wherein highly conducting nano-sized (mesoporous), high surface area activated carbon (NCB) was mixed with the electrode-active material in addition to the conventional acetylene black (AB) carbon. Interestingly, when tested against lithium in a half-cell the cycling characteristics of the materials improved as a result of an intimate contact between the active grains (grain-grain contact) and better electrolyte wetting into the pores leading to an overall enhancement in the conductivity. Accordingly, the capacity offered by the materials

followed an increasing trend. The following section gives a detailed description of the formation nano-composites and the results obtained for conductivity enhancement.

5. Formation of nano-composite electrodes and improved electrochemical properties of polyanion cathode materials

5.1 Preparation of nano-composite electrodes

Nano-composite positive electrodes (cathode) consisted of 65% active material, 5% binder (PTFE) and 30% conducting carbon mixture. The conducting carbon mixture comprised an equal proportion of acetylene black (AB) [BET surface area: 394 m^2/g; Grain size: 0.1 μm -10 μm; σ_e: 10.2 S/cm] and NCB (nano-sized particles exhibiting mesoporosity of 3-10 nm; Monarch 1400, Cabot Inc, USA, BET surface area: 469 m^2/g; Grain size: 13 nm; σ_e; 19.7 S/cm). The nano-composite electrodes were fabricated following the usual procedure.

5.2 Modification in the electrochemical properties of polyanion cathode materials

To investigate the effect of nano-sized carbon black on the electrochemical behaviour of all the four materials, nano-composite cathode/Li half-cells were tested galvanostatically under the same experimental conditions.

The first charge/discharge curves obtained using the nano-composite positive electrodes ($Li_2M_2(MoO_4)_3$) were compared to the first charge/discharge curves of the conventional electrode (without NCB) as shown in Fig. 13.

Fig. 13 shows a clear evidence for the difference between the two cases in terms of IR drop, the amount of lithium removal/insertion and shape of the discharge profiles. The reduced IR (ohmic) drop at the beginning of the discharge process after charge in the case of the nano-composite electrodes is well seen in Fig 13 (inset). But, in the conventional case, a large IR (ohmic) drop was observed. As for the $Li_2Ni_2(MoO_4)_3$ nano-composite electrode, we obtained a first discharge capacity of 86 mAh/g down to 2.0 V which is approximately a four fold excess compared to the conventional electrode where the discharge capacity was 26 mAh/g down to 2.0 V. A first discharge capacity of 55 mAh/g was obtained in the case of $Li_2Co_2(MoO_4)_3$ nano-composite electrode which is 2.5 timer higher in comparison with the conventional type $Li_2Co_2(MoO_4)_3$ electrode.

Apart from the above changes observed, a smooth discharge profile of the nano-composite electrode right from the beginning down to 2.0 V is note worthy; whereas the conventional electrode seems to exhibit two-slope feature during the first discharge that appears distinctly on the discharge plateau. These significant changes observed in the discharge profile clearly demonstrate the role of non-graphitized carbon black (nano-sized) on the electrochemical properties of the host cathode.

We compared the first discharge/charge curves obtained using the nano-composite positive electrodes ($Li_xM_2(MoO_4)_3$) with the first discharge/charge curves of the conventional electrodes as shown in Fig. 14.

It is noticeable from Fig. 14a that there is dissimilarity between the two cases in terms of IR (ohmic) drop even though the discharge/charge profiles look alike. In the usual case, IR drop at the beginning of the discharge process was large and the discharge profile was found to proceed vertically down to 2.7 V from OCV (3.5 V) without any quantitative lithium insertion reaction. This is due to a very low electronic conductivity of polyanion

materials which is a common intricacy preventing the polyanions from practical use. On the other hand, much minimized IR drop in the case of the nano-compoiste electrode is

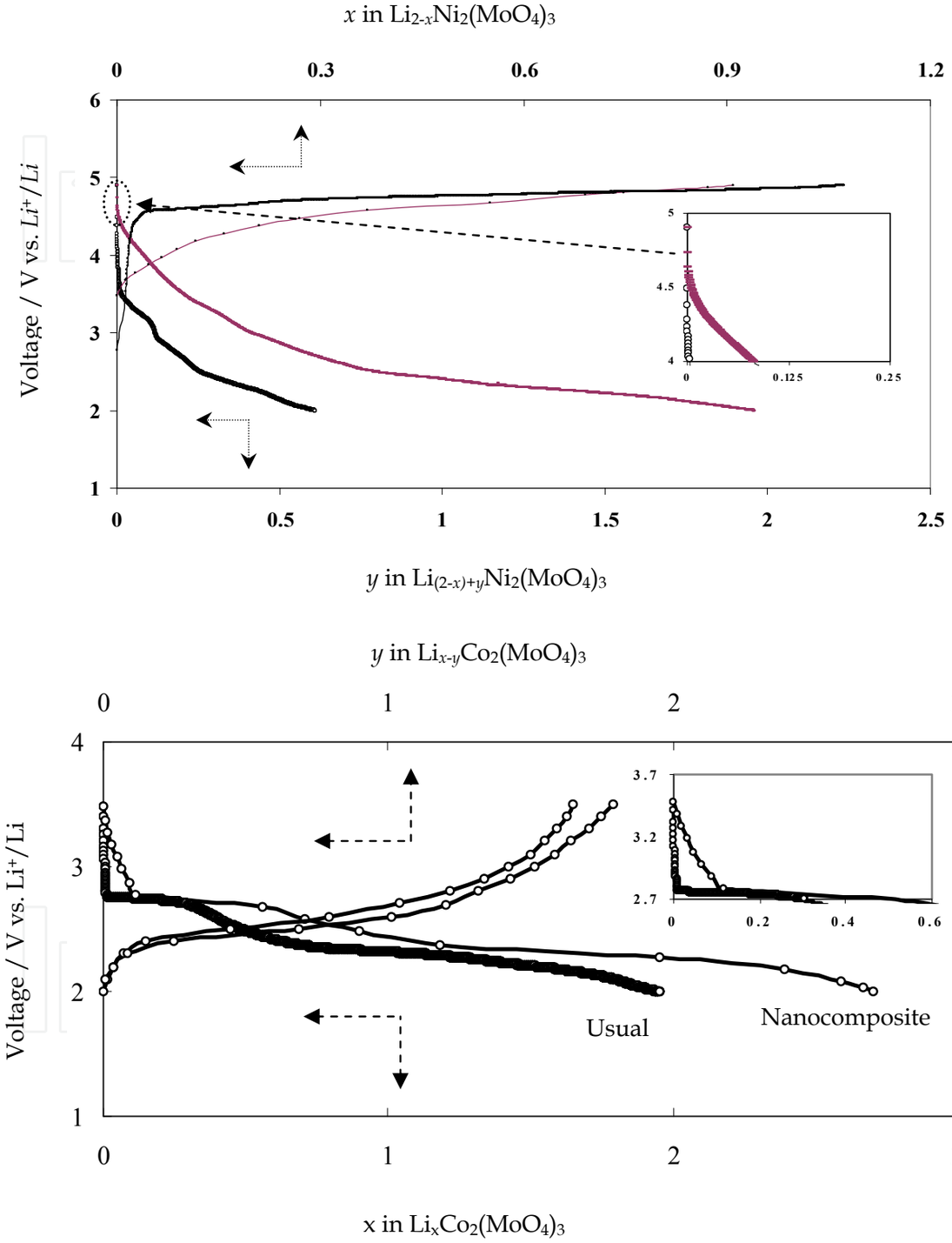

Fig. 13. Comparison of first charge/discharge of nano-composite and conventional $Li_2M_2(MoO_4)_3$ against lithium between 4.9 and 1.5 V. (Prabaharan et al., 2006).

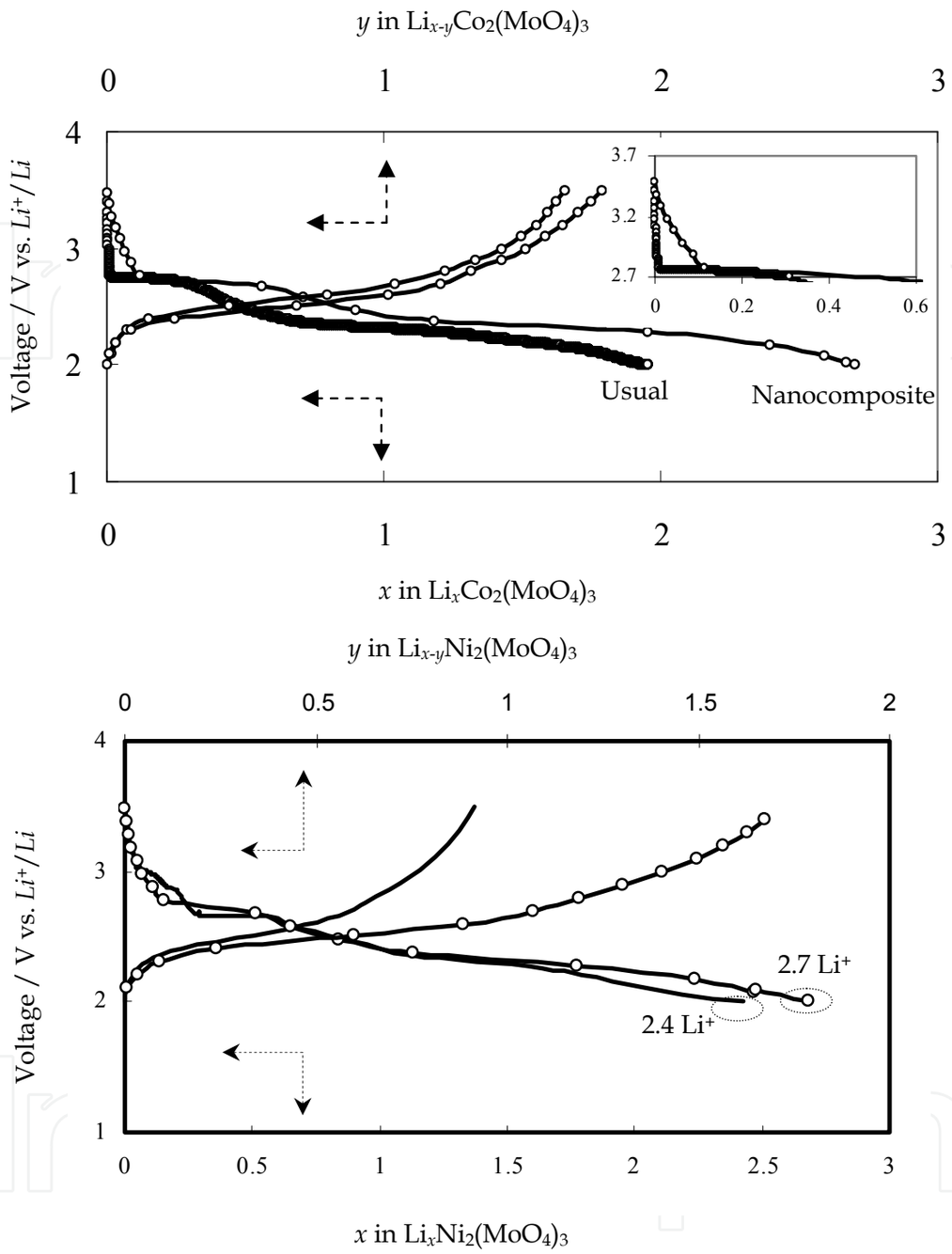

Fig. 14. Comparison of first charge/discharge of nano-composite and conventional $Li_xM_2(MoO_4)_3$ against lithium between 3.5 and 2.0 V. (Prabaharan et al., 2004, 2007, 2008).

well evident in Fig. 14a (inset) and the discharge profile was observed to exhibit an exponential decay with a progressive insertion of lithium in the electrode. Furthermore, there is a difference between the two cases in the amount of lithium insertion during discharge. About 2.7 Li^+ was inserted in the nano-composite electrode corresponding to the first discharge capacity of 121 mAh/g. This value is larger than the capacity obtained from

the conventional composite electrode added with acetylene black (87 mAh/g for 1.95 Li^+ down to 2.0 V).

As for the $Li_xNi_2(MoO_4)_3$, the first discharge/charge curves corresponding to the usual and nano-composite electrodes are distinct concerning the discharge capacity and not the IR drop (Fig. 14b). Usual $Li_xNi_2(MoO_4)_3$ delivered 108 mAh/g as its first discharge capacity, but nano-composite $Li_xNi_2(MoO_4)_3$ gave rise to a first discharge capacity of 120 mAh/g. Although the nano-composite $Li_xNi_2(MoO_4)_3$ indicated better discharge/charge characteristics than the usual $Li_xNi_2(MoO_4)_3$, we could observe that the performance is not comparable to the level of enhancement in the nano-composite $Li_xCo_2(MoO_4)_3$. We ascribed the variation in the electrochemical performance as due to the variation in the grain size.

It is apparent that the role of NCB is significant in modifying the discharge/charge profiles with much improvement. The vital role of nano-sized high surface area activated carbon in improving the electrochemical properties of the positive electrode is implicit through these prominent variations monitored in the discharge profile. Presence of NCB in the electrode increased the electronic conductivity by enhancing the intactness between the active grains.

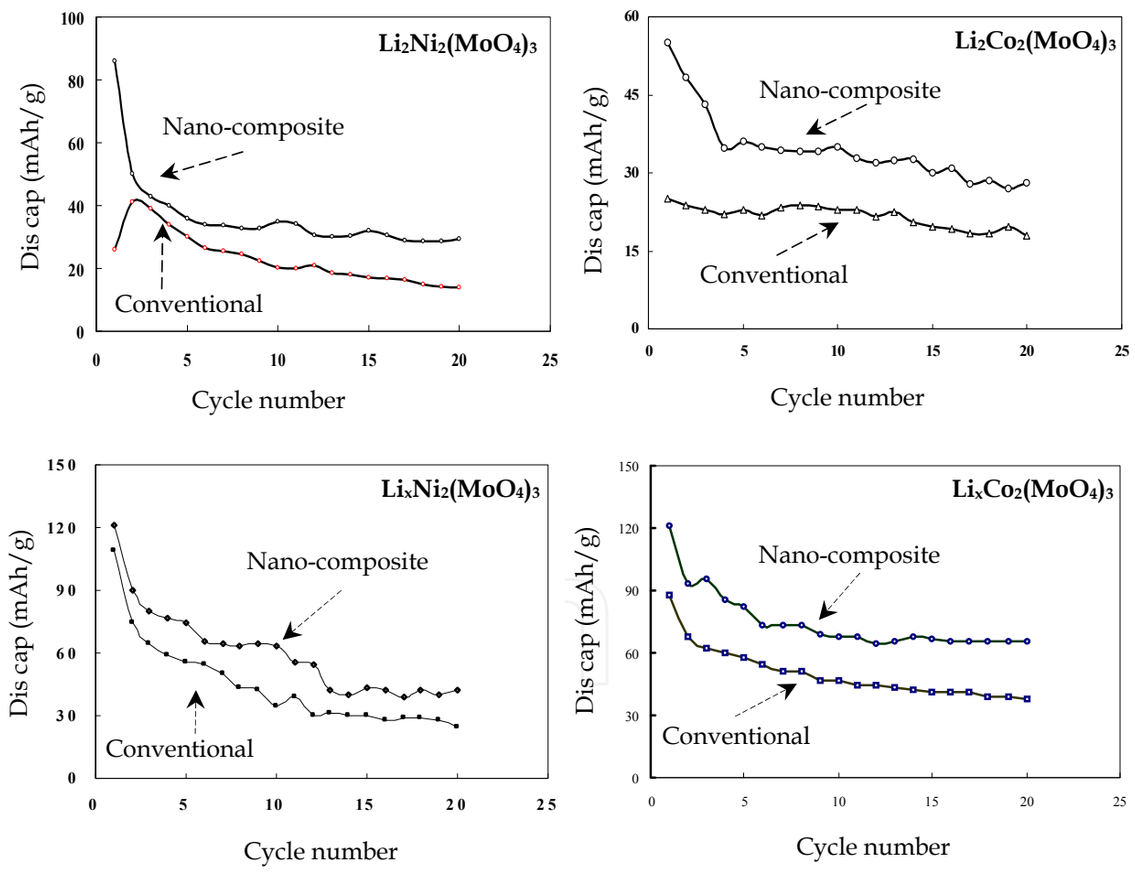

Fig. 15. Discharge capacity of conventional and nano-composite electrodes vs. cycle number

With an aspiration to examine the effect of mesoporous carbon during prolonged cycling, we carried out multiple cycling tests on the test cells for the first twenty cycles under the same experimental conditions. The amount of lithium inserted into the nano-composite

electrode during discharge was larger than that in the conventional electrode for all the twenty cycles studies in all the four cases. Besides this, the charge profiles also showed significant improvement, which would certainly help inserting more lithium in the subsequent discharge. The results are summarized in the form of variation of discharge capacity vs. cycle number. The variation in the discharge capacity with cycle number corresponding to the usual and nano-composite $Li_2M_2(MoO_4)_3$ and $Li_xM_2(MoO_4)_3$ are shown in Fig. 16.

	Electrochemical properties of $Li_2Ni_2(MoO_4)_3$ electrode			
	Conventional cathode		Nano-composite cathode	
Cycle no.	Amount of Li^+ inserted down to 2.0 V	Discharge capacity (mAh/g)	Amount of Li^+ inserted down to 2.0 V	Discharge capacity (mAh/g)
1	0.6	26	2	86
5	0.7	30	0.8	36
10	0.5	20	0.78	35
15	0.4	17	0.72	32
20	0.3	14	0.7	29

Table 1. Enhanced electrochemical properties of nano-composite $Li_2Ni_2(MoO_4)_3$ electrode compared to conventional $Li_2Ni_2(MoO_4)_3$ electrode.

	Electrochemical properties of $Li_2Co_2(MoO_4)_3$ electrode			
	Conventional cathode*		Nano-composite cathode**	
Cycle no.	Amount of Li^+ inserted down to 2.0 V	Discharge capacity (mAh/g)	Amount of Li^+ inserted down to 2.0 V	Discharge capacity (mAh/g)
1	0.53	23	1.25	55
5	0.522	22.9	0.8	36
10	0.52	22.8	0.79	35
15	0.45	19.7	0.69	30
20	0.4	17.8	0.64	28

Table 2. Enhanced electrochemical properties of nano-composite $Li_2Co_2(MoO_4)_3$ electrode compared to conventional $Li_2Co_2(MoO_4)_3$ electrode.

The observed improvement with regard to electrochemical properties of NCB added positive composite electrodes over the conventional electrodes with mere acetylene black are summarized in Tables 1, 2, 3 and 4 for all the four cases. It is obvious from the tables that NCB added positive electrodes exhibit improved extended cycling characteristics. The nano-sized grains accompanied by the presence of meso porosity in the NCB could have facilitated the enhanced grain-grain contact between the electrode active particles and provided the enhanced intactness between electrode active grains and the conductive additive carbons established via PTFE upon repeated charge/discharge cycles.

	Electrochemical properties of $Li_xNi_2(MoO_4)_3$ electrode			
	Conventional cathode*		Nano-composite cathode**	
Cycle no.	Amount of Li^+ inserted down to 2.0 V	Discharge capacity (mAh/g)	Amount of Li^+ inserted down to 2.0 V	Discharge capacity (mAh/g)
1	2.42	109	2.68	121
5	1.24	55.5	1.66	70
10	0.78	40	1.4	63
15	0.68	34	0.95	43
20	0.57	28	0.92	42

Table 3. Enhanced electrochemical properties of nano-composite $Li_xNi_2(MoO_4)_3$ electrode compared to conventional $Li_2Ni_2(MoO_4)_3$ electrode.

	Electrochemical properties of $Li_xCo_2(MoO_4)_3$ electrode			
	Conventional cathode*		Nano-composite cathode**	
Cycle no.	Amount of Li^+ inserted down to 2.0 V	Discharge capacity (mAh/g)	Amount of Li^+ inserted down to 2.0 V	Discharge capacity (mAh/g)
1	1.95	87	2.7	121
5	1.3	58	1.9	85
10	1	44	1.6	73
15	0.9	41	1.5	66
20	0.8	37	1.5	66

Table 4. Enhanced electrochemical properties of nano-composite $Li_xCo_2(MoO_4)_3$ electrode compared to conventional $Li_2Ni_2(MoO_4)_3$ electrode.

5. Conclusion

We identified a group of NASICON open framework structured polyanion materials and examined the materials for rechargeable lithium battery application. We found that the open framework structure of these materials facilitated easy insertion/extraction of lithium into/from their structure. We synthesized the materials in lithium-rich $[Li_2M_2(MoO_4)_3]$ and lithium-free $[Li_xM_2(MoO_4)_3]$ (M= Ni, Co) phases, for the first time, by means of a low temperature soft-combustion technique. The soft-combustion synthesis usually yields single-phase materials with high phase purity and is suitable for bulk preparation of battery grade electrode powders. The materials were characterized for structure, morphology and electrochemical lithium insertion/extraction kinetics and the results were presented and discussed in the light of XRD, SEM and electrochemical techniques in relation to the electrode-active character of the materials.

All the materials were found to crystallize in a single phase structure with submicron sized particles. The electrode-active behavior of the new materials was examined in a two-electrode configuration utilizing a Li^+ non-aqueous environment. Both the systems were

found to exhibit electrochemically reversibility as evidenced from Slow Scan Cyclic Voltammetry (SSCV) studies. As for the lithium-rich phases, $Li_2M_2(MoO_4)_3$, the charge-discharge profiles obtained by means of Galvanostatic cycling tests between 4.9 V and 1.5 V signified removal/reinsertion of lithium in the new materials with good discharge capacity. The Galvanostatic discharge/charge tests conducted between 3.5 and 1.5 V corresponding to the lithium-free phases, $Li_xM_2(MoO_4)_3$ also indicated the reversibility of the materials.
During extended cycling, structural disruption of the materials was evidenced from the shape of the cycling profiles regardless of the initial phase of the materials. The discharge capacity was found to decrease during prolonged cycling due to a very low lattice conductivity of the polyanaion systems.
We applied a novel and efficient nano-composite approach to boost the surface conductivity of the polyanion materials by introducing a nano-sized mesoporous carbon black (NCB). We found that the high surface area carbon could increase the intactness between the electrode-active grains much more effectively leading to increased conductivity of the electrode material on the whole. Consequently, we proved that the nano-composite approach is very effective in improving the electrochemical characteristics of the group of new materials taken for the present investigation with a substantial enhancement in discharge capacity.

6. References

Alvarez-Vega, M.; Amador, U. & Arroyo-de Dompablo, ME. (2005). Electrochemical Study of $Li_3Fe(MoO_4)_3$ as Positive Electrode in Lithium Cells. *Journal of the Electrochemical Society,* vol. 152, no. 7, pp. A1306-A1311.

Arroyo-de Dompablo, ME.; Alvarez-Vega, M.; Baehtz, C. & Amador, U. (2006). Structural Evolution of $Li_{3+x}Fe(MoO_4)_3$ upon Lithium Insertion in the Compositional Range $0 \leq x \leq 1$. *Journal of the Electrochemical Society,* vol. 153, no. 2, pp. A275-A281.

Barker, J.; Saidi, MY. & Swoyer, J.L. (2003). Electrochemical insertion properties of the novel lithium vanadium fluorophosphates. *Journal of the Electrochemical Society*, 150 (10), A1394-A1398.

Begam, KM.; Michael, MS.; Taufiq-yap, Y.H. & Prabaharan, S.R.S. (2004). New lithiated NASICON-type $Li_2Ni_2(MoO_4)_3$ for rechargeable batteries: Synthesis, structural and electrochemical properties. *Electrochemical and Solid State Letters*, vol. 7, no. 8, pp. A242-246.Begam, KM.; Michael, M.S. & Prabaharan, S.R.S. (2004). Topotactic Lithium Insertion/Extraction Properties of a New Polyanion Material, $Li_xCo_2(MoO_4)_3$ [$0 \leq x < 3$] for rechargeable lithium batteries. Proceedings of the 9th Asian Conference on Solid State Ionics, pp. 461-468, ISBN 981-238-932-6, South Korea, June 2004, World Scientific, Singapore.

Begam, KM.; Selladurai, S.; Michael, M;.S. & Prabaharan, S.R.S. (2004). Synthesis and redox behavior of a new polyanion compound, $Li_2Co_2(MoO_4)_3$ as 4-V class positive electrode material for rechargeable lithium batteries. J*ournal of Ionics*, vol. 10, pp. 77-83.

Begam, KM.; Taufiq-Yap, YH.; Michael, MS. & Prabaharan, S.R.S. (2004). A new NASCON-type polyanion, $Li_xNi_2(MoO_4)_3$ as 3-V class positive electrode material for rechargeable lithium batteries. *Solid State Ionics*, vol. 172, pp. 47-52.

Begam, KM, & Prabaharan, S.R.S. (2006). Effect of mesoporous carbon black on the cycling characteristics of $Li_2Co_2(MoO_4)_3$ for lithium batteries. Proceedings of the 10th Asian Conference on Solid State Ionics, pp. 313-320, ISBN 981-256-877-8, Srilanka, June 2006, World Scientific, Singapore.

Begam, KM, & Prabaharan, S.R.S. (2006). Improved cycling performance of nano-composite $Li_2Ni_2(MoO_{4)3}$ as a lithium battery cathode material. *Journal of Power Sources*, vol. 159, pp. 319-322.

Begam, KM.; Michael, M.S. & Prabaharan, S.R.S. (2007). Enhancd cycling properties of transition metal molybdates, $Li_xM_2(MoO_4)_3$ {0≤x<3} [M = Co, Ni]: a nono-composite appraoch for lithium batteries. *Journal of Ionics*, vol. 13, pp. 467-471.

Begam, KM.; Michael, M.S. & Prabaharan, S.R.S. (2008). Nanostructured lithium-free oxyanion cathode, $Li_xCo_2(MoO_4)_3$ [0≤x<3] for 3 V class lithium batteries. *J Solid State Electrochem.* Vol. 12, pp. 971-977.

Bykov, AB.; Chirkin, AP.; Demyanets, LN.; Doronin, S.N. & Muradyan, L.N. (1990). Superionic conductors $Li_3M_2(PO_4)_3$ (M=Fe, Sc, Cr): Synthesis, structure and electrophysical properties. *Solid State Ionics*, vol. 38, no. 1-2, pp. 31-52.

Chung, SY.; Blocking, JT. & Chiang, Y.M. (2002). Electronically conductive phospho-olivines as lithium storage electrodes. *Nature materials*, vol. 1, pp. 123-128.

Davis, RJ.; Hobson, MJ.; Macklin, WJ. & Neat, RJ. (2004). Vanadium phosphate glasses. Effect of composition on their structure and performance as cathodes in high-temperature lithium polymer-electrolyte cells. *J. Mater. Chem.* Vol. 4, pp. 113-118.

Gaubicher, J.; Wurm, C.; Goward, G.; Masquelier, C. & Nazar, L.F. (2000). Rhombohedral form of $Li_3V_2(PO_4)_3$ as a cathode in Li-ion batteries. *Chemistry of Materials,* vol. 12, no. 11, pp. 3240-3242.

Goodenough, JB.; Hong, HYP. & Kafalas, JA. (1976). Fast Na^+ ion transport in skeleton structures. *Materials Research Bulletin*, vol. 11, no. 2, pp. 203-247.

Harrison, WTA.; Chowdary, U.; Machiels, CJ.; Sleight, AW. & Cheetam, AK. (1985). Preparation of ferric tungstate and its catalytic behavior toward methanol. *Journal of Solid State Chemistry*, vol. 60, no. 1, pp. 101-106.

Hirano, A.; Kanno, R.; Takeda, Y. & Yamaguchi, Y. (1995). Relationship between non-stoichiometry and physical properties in $LiNiO_2$. *Solid State Ionics*, vol. 78, pp. 123-131.

Hong, HYP. (1976). Crystal structure and crystal chemistry in the system $Na_{1+x}Zr_2Si_xP_{3-x}O_{12}$. *Materials Research Bulletin*, vol. 11, no. 2, pp. 173-182.

Huang, H.; Yin, SC. & Nazar, LF. (2001). Approaching theoretical capacity of $LiFePO_4$ at room temperature at high rates. *Electrochemical and Solid-State Letters*, vol. 4, no. 10, pp. A170-A172.

Huang, H.; Yin, SC.; Kerr, T; Taior, N. & Nazar, LF. (2002). Nanostructured Composites: A High Capacity, Fast Rate $Li_3V_2(PO_4)_3$/Carbon Cathode for Rechargeable Lithium Batteries (p 1525-1528)*Adv. Mater*. Vo. 14, pp. 1525-1528.

Koboyashi, H.; Shigemura, H.; Tabuchi, M.; Sakaebe, H.; Ado, K. & Kagayama, H. (2000). Electrochemical properties of hydrothermally obtained $LiCo_{1-x}Fe_xO_2$ as a positive electrode material for rechargeable lithium batteries. *Journal of the Electrochemical Society,* vol. 147, no. 3, pp. 960-969.

Long GJ.; Longworth G.; Battle P.; Cheetham AK.; Thundathil RV. & Beveridge D. (1979). A study of anhydrous iron (III) sulfate by magnetic susceptibility, Mossbauer and neutron diffraction techniques. *Inorganic Chemistry*, vol. 18, no. 3, pp. 624-632.

Manthiram, A. & Goodenough, JB. (1987). Lithium insertion into $Fe_2(MoO_4)_3$ frameworks: Comparison of M=W with M=M*. *Journal of Solid State Chemistry,* vol. 71, pp. 349-360.

Manthiram, A. & Goodenough, JB. (1989). Lithium insertion into $Fe_2(SO_4)_3$ frameworks. *Journal of Power Sources*, vol. 26, pp. 403-409.

Morcrette, M.; Leriche, JB.; Patoux, S.; Wurm, C. & Masquelier, C. (2003). In situ X-ray diffraction during lithium extraction from rhombohedral and monoclinic $Li_3V_2(PO_4)_3$. *Electrochemical and Solid State Letters,* vol. *6*, no. 5, pp. A80-A84.

Moshtev, RV.; Zlatilova, P.; Manev, P. & Sato, A. (1995). The $LiNiO_2$ solid solution as a cathode material for rechargeable lithium batteries. *Journal of Power Sources*, vol. 54, pp. 329-333.

Nadiri, A.; Delmas, C.; Salmon, R. & Hagenmullar, P. (1984). J. Rev. Chim.Miner, vol. 21, pp. 83.

Nanjundasamy, KS.; Padhi, AK.; Goodenough, JB.; Arai, H. & Yamaki, J. (1996). Synthesis, redox potential evaluation and electrochemical characteristics of NASICON-related-3D framework compounds. *Solid State Ionics*, vol. 92, pp. 1-10.

Nazar, L.; Huang, H.; Yin, S.C. & Kerr, T. (2002). Transition metal phosphates as positive electrodes for Li-ion batteries-Structure, microstructure and properties.

Proceedings of 11th International meeting on lithium batteries, 212, Monterey, CA.

Okada, S. (1996). *International Symposium on lithium batteries*, P19. Tokyo.

Ozima, M.; Sato, S. & Zoltai, T. (1977). The crystal structure of a lithium-nickel molybdate, $Li_2Ni_2Mo_3O_{12}$, and the systematics of the structure type. Acta Crystallographica, vol. B33, pp. 2175-2181.

Padhi, AK.; Nanjundasamy, KS, & Goodenough, JB. (1997). Phospho-olivines as positive electrode materials for rechargeable lithium batteries. *Journal of the Electrochemical Society*, vol. 144, no. 4, pp. 1188-1194.

Padhi, AK.; Nanjundasamy, KS.; Masquelier, C. & Goodenough, JB. (1997). Mapping of transition metal redox energies in phosphates with NASICON structure by lithium intercalation. *Journal of the Electrochemical Society*, vol. 144, no. 8, pp. 2581-2586.

Padhi, AK.; Manivannan, V. & Goodenough, J.B. (1998). Tuning the position of the redox couples in materials with NASICON structures by anionic substitution. *Journal of the Electrochemical Society,* vol. 145, no. 5, pp. 1518-1520.

Patoux, S.; Wurm, C.; Morcrette, M.; Rousse, G. & Masquelier, C. (2003). A comparative structural and electrochemical study of monoclinic $Li_3Fe_2(PO_4)_3$ and $Li_3V_2(PO_4)_3$. Journal of Power Sources, vol. 119-121, pp. 278-284.

Prabaharan, SRS.; Ramesh, S.; Michael, MS. & Begam, KM. (2004). Characterization of soft-combustion-derived NASICON-type $Li_2Co_2(MoO_4)_3$ for lithium batteries. *Materials Chemistry and Physics*, vol. 87, pp. 318-326.

Prabaharan, SRS.; Fauzi, A.; Michael, MS. & Begam, KM. (2004). New NASICON-type $Li_2Ni_2(MoO_4)_3$ as a positive electrode material for rechargeable lithium batteries. *Solid State Ionics*, vol. 171, pp. 157-165.

Prabaharan, SRS.; Michael, MS.; Ramesh, S., & Begam, K.M. (2004). Synthesis and redox properties of $Li_xNi_2(MoO_4)_3$: a new 3-V class positive electrode material for rechargeable lithium batteries. *Journal of Electroanalytical Chemistry,* vol. 570, pp. 107-112.

Prabaharan, SRS.; Michael, MS. & Begam, K.M. (2004). Synthesis of a polyanion cathode material, $Li_2Co_2(MoO_4)_3$ and its electrochemical properties for lithium batteries. *Electrochemical and Solid State Letters*, vol. 7, no. 11, pp. A416-A420.

Reiff, WM.; Zhang, JH. & Torardi, CC. (1986). Topochemical lithium insertion into $Fe_2(MoO_4)_3$: structure and magnetism of $Li_2Fe_2(MoO_4)_3$. *Journal of Solid State Chemistry*, vol. 62, pp. 231-240.

Reimers, J.N. & Dahn, J.R. (1992). Electrochemical and in situ X-ray diffraction studies of lithium intercalation in Li_xCoO_2. *Journal of the Electrochemical Society,* vol. 139, no. 8, pp. 2091-2096.

Saidi, MY.; Barker, J.; Huang, H.; Swoyer, J.L. & Adamson, G. (2002). Performance characteristics of lithium vanadium phosphate as a cathode material for lithium-ion batteries. *Journal of Power Sources,* vol. 119-121, pp. 266-272.

Saidi, MY.; Barker, J.; Huang, H.; Swoyer, J.L. & Adamson, G. (2002). Electrochemical properties of lithium vanadium phosphate as a cathode material for lithium-ion batteries. *Electrochemical and Solid State Letters,* vol. 5, no. 7, pp. A149-A151.

Sato, M.; Ohkawa, H.; Yoshida, K.; Saito, M. & Toda, K. (2000). Enhancement of discharge capacity of $Li_3V_2(PO_4)_3$ by stabilizing the orthorhombic phase at room temperature. *Solid State Ionics,* vol. 135, no. 1-4, pp. 137-142.

Tarascon, JM. & Armand, M. (2001). Issues and challenges facing rechargeable lithium batteries. *Nature,vol.* 414, pp. 359-367.

Torardi, CC. & Prince, A. (1986). Structure of the lithium insertion compound $Li_2Fe_2(MoO_4)_3$ from neutron powder diffraction data. *Materials Research Bulletin*, vol. 21, no. 6, pp. 719-726.

Wang, GX.; Bradhurst, DH.; Dou, SX. & Liu, HK. (2003). $LiTi_2(PO_4)_3$ with NASICON-type structure as lithium-storage materials. Journal of Power Sources, vol. 124, pp. 231-236.

Yang, S.; Song, Y.; Zavali, PY. & Whittingham, M.S. (2002). Reactivity, stability and electrochemical behavior of lithium iron phosphate. *Electrochemistry Communications*, vol. 4, pp. 239-244.

Yin, SC.; Grondey, H.; Strobel, P.; Huang, H. & Nazar, LF. (2003). Charge ordering in lithium vanadium phosphates: Electrode materials for lithium ion batteries. J. Am. Chem.Soc. vol. 125, pp. 326-327.

Zhang, D.; Tong, Z.; Xu, G.; Li, S. & Ma, J. (2009). Template fabrication of $NiFe_2O_4$ nanorods; Characterization, magnetic and electrochemical properties. *Solid State Sciences*, vol. 11, pp. 113-117.

Zhu, XJ.; Liu, YX.; Geng, LM. & Chen, LB. (2008). Synthesis and performance of lithium vanadium phosphate as cathode materials for lithium ion batteries by a sol-gel method. *Journal of Power Sources*, vol. 184, pp. 578-582.

IntechOpen

IntechOpen

Lithium-ion Batteries

Edited by Chong Rae Park

ISBN 978-953-307-058-2
Hard cover, 132 pages
Publisher InTech
Published online 01, April, 2010
Published in print edition April, 2010

There have been numerous excellent books on LIBs based on various different viewpoints. But, there is little book available on the state of the art and future of next generation LIBs, particularly eventually for EVs and HEVs. This book is therefore planned to show the readers where we are standing on and where our R&Ds are directing at as much as possible. This does not mean that this book is only for the experts in this field. On the contrary this book is expected to be a good textbook for undergraduates and postgraduates who get interested in this field and hence need general overviews on the LIBs, especially for heavy duty applications including EVs or HEVs.

How to reference

In order to correctly reference this scholarly work, feel free to copy and paste the following:

K.M. Begam, M.S. Michael and S.R.S. Prabaharan (2010). NASICON Open Framework Structured Transition Metal Oxides for Lithium Batteries, Lithium-ion Batteries, Chong Rae Park (Ed.), ISBN: 978-953-307-058-2, InTech, Available from: http://www.intechopen.com/books/lithium-ion-batteries/nasicon-open-framework-structured-transition-metal-oxides-for-lithium-batteries

INTECH
open science | open minds

InTech Europe
University Campus STeP Ri
Slavka Krautzeka 83/A
51000 Rijeka, Croatia
Phone: +385 (51) 770 447
Fax: +385 (51) 686 166
www.intechopen.com

InTech China
Unit 405, Office Block, Hotel Equatorial Shanghai
No.65, Yan An Road (West), Shanghai, 200040, China
中国上海市延安西路65号上海国际贵都大饭店办公楼405单元
Phone: +86-21-62489820
Fax: +86-21-62489821

© 2010 The Author(s). Licensee IntechOpen. This chapter is distributed under the terms of the Creative Commons Attribution-NonCommercial-ShareAlike-3.0 License, which permits use, distribution and reproduction for non-commercial purposes, provided the original is properly cited and derivative works building on this content are distributed under the same license.

IntechOpen

IntechOpen